

A comparison of the accuracy of two types of instrumentation for measuring vertical wheel load

P. A. LEBLANC, MAsC, Research Officer, National Research Council of Canada, J. H. F. WOODROOFFE, MAsC, Research Officer, National Research Council of Canada, and A. T. PAPAGIANNAKIS, PhD, Professor, Memorial University of Newfoundland, Canada

Studies of pavement loading by heavy vehicles make use of on-board instrumentation that is necessarily remote from the tire/pavement contact patch. Several instrumentation techniques have been developed to measure vertical wheel load. In this paper, the accuracy of two types are compared. The comparison involves static and dynamic calibrations performed on a servo-hydraulic shaker facility for heavy vehicles, and road tests conducted with an instrumented experimental vehicle.

NOMENCLATURE

d	Distance between wheel load centroid and section A	m
i	Subscript identifying left and right wheels	-
I_c	Mass moment of inertia of m about its centroid	kgm ²
l	Distance between axle accelerometers	m
L	Wheel load	kN
L_{bi}	Wheel load measured by bending-moment transducer	kN
L_{ci}	Load measured by load-cell	kN
L_{ri}	Reference wheel load	kN
L_{si}	Wheel load measured by shear-force transducer	kN
m, m_i	Mass outboard of the strain gauges	kg
m_p	Mass of wheel platform	kg
M	Bending moment at section A	Nm
V	Shear force at section A	kN
\bar{y}	Distance between the centroid of m and section A	m
\bar{Y}	Distance between the centroid of m and axle centre	m
$\ddot{z}_c, \ddot{z}_{ci}$	Vertical acceleration at the centroid of m	m/s ²
\ddot{z}_i	Vertical acceleration measured by axle accelerometer	m/s ²
\ddot{z}_{pi}	Vertical acceleration measured by platform accelerometer	m/s ²
$\ddot{\theta}$	Angular acceleration of m	rad/s ²

1.0 Introduction

The work reported in this paper constitutes the initial phase of NRC's Heavy Vehicle Suspension Project. The objective of the Project is to develop a cost-effective test method for evaluating the performance of heavy vehicle suspension systems as related to pavement damage. Ideally, the role of the performance evaluation method will be to assign maximum allowable static loads to suspension systems based on their performance. This approach would permit a technical measure of "acceptability" for suspension systems, and would assist manufacturers and regulators in developing and promoting road-friendly suspensions.

NRC's Heavy Vehicle Suspension Project constitutes Canada's commitment to an international research programme which seeks to address the numerous aspects of the problem of vehicle-generated pavement damage. The program is co-ordinated by a scientific expert group assembled under the Organization for Economic Cooperation and Development (OECD). Fourteen countries are participating in the research programme, bringing together expertise from vehicle dynamics and pavement technology, and from the emerging discipline of vehicle/pavement interaction.

Although NRC's Heavy Vehicle Suspension Project is closely linked to, and will definitely benefit from, the OECD co-ordinated research programme, it is designed to produce concrete results on its own. Its ultimate purpose is to help governments in Canada reduce the cost of maintaining the road infrastructure. A significant portion of this cost is directly attributable to pavement damage caused by heavy vehicle wheel loads, that is, the vertical forces generated at the tire/pavement interface. The magnitude of these wheel loads is highly dependent on the type of suspension systems in use (ref. 1, 2), and this forms the underlying reason for the suspension project.

The first phase of NRC's Project, reported in this paper, evolved from what was initially scheduled to be a "routine" calibration of the wheel load instrumentation on NRC's experimental vehicle. However, unsatisfactory calibration results were obtained which raised doubts about the validity of the wheel load instrumentation. This in turn led to the development, calibration, and comparison of accuracy of two types of instrumentation for measuring wheel loads.

2.0 Previously Developed Wheel Load Transducers

Several different types of on-board wheel load measuring systems have been developed in the past three decades. A few of these are described below.

Three types of on-board wheel load measuring systems were evaluated by Whittemore et al. (ref. 3). They included a differential tire pressure transducer, a strain-gauged axle housing transducer, and a strain-gauged wheel transducer. Tests conducted by driving an instrumented axle over an embedded weigh scale revealed that the tire pressure transducer suffered from nonlinearity and phase-shift between tire pressure and wheel load. The amplitude of tire pressure was also shown to change with frequency when excited with a constant wheel load amplitude.

Tests conducted on a servo-hydraulic shaker facility, and road tests conducted by driving an instrumented truck over an embedded weigh scale, showed that both the strain-gauged axle housing transducer and the strain-gauged wheel transducer systems produced very good results (ref. 3).

A fourth possible method for measuring wheel loads consists of measuring tire deflection. This approach was used by Cantieni (ref. 4) who used infra-red transmitters and receivers to measure tire deflection which was subsequently converted into wheel load.

Woodrooffe et al. used a strain-gauged axle housing transducer to measure dynamic wheel load during their heavy vehicle suspension study (ref. 2). This instrumentation was similar to that used by Whittemore except that strain-gauges sensitive to bending moment were used, as opposed to strain-gauges sensitive to shear force.

From the standpoint of ensuring measurement accuracy and because a total of ten dual wheels need to be instrumented, the strain-gauged axle housing transducers were found to be the most appealing type of wheel load instrumentation for the NRC Project.

The tire pressure transducers simply do not provide the required accuracy. The main disadvantage of tire-deflection-based transducers, similar to the one used by Cantieni, is that they must be calibrated while the tire is rolling, because the stiffness and damping characteristics of rolling tires are different than those of tires which are not rolling (ref. 3). Finally, the main disadvantage with the strain-gauged wheel transducer is its complexity and high cost.

3.0 Strain-Gauged Axle Housing Transducers

The concept of measuring wheel load by strain-gauging the axle housing was first developed by Hopkins and Boswell (ref. 5). This measurement technique was later improved at the General Motors Proving Ground by the installation of an accelerometer on the axle to account for an inertial force component (see additional details below). The improved method was subsequently adapted by Whittemore et al. and Woodrooffe et al. in their respective studies.

The theory behind the strain-gauged axle housing transducers is derived from conditions of dynamic equilibrium of the free body diagram of the wheel and axle stub shown in Figure 1. The derivation of the governing equations is based on rigid body theory and on the assumption of small angles, that is, $\sin \theta$ and $\cos \theta$ are approximated as θ and 1, respectively.

The wheel load measurement method adopted by Whittemore is based on dynamic equilibrium of the vertical forces acting on the mass outboard of the strain-gauges, namely,

$$L + m\ddot{z}_c - V = 0 \tag{1}$$

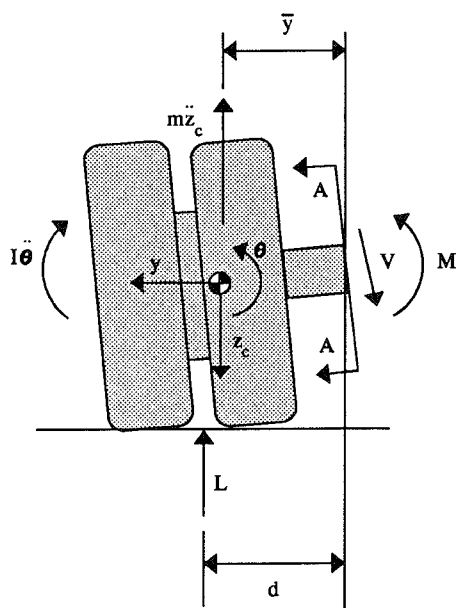


Fig. 1. Free body diagram of dual wheel and axle stub

where L is the wheel load, m is the mass outboard of the strain gauges, \ddot{z}_c is the vertical acceleration at the centroid of m , and V is the shear force at section A. The wheel load instrumentation based on Equation 1 will be referred to as the shear-force transducer.

The wheel load measurement method adopted by Woodrooffe et al. is based on dynamic equilibrium of the moments acting on the mass outboard of the strain-gauges. The sum of the moments about the centroid of section A leads to the following equation:

$$Ld + m\ddot{z}_c\bar{y} + I_c\ddot{\theta} - M = 0 \tag{2}$$

where d is the distance between the centroid of the wheel load and section A, \bar{y} is the distance between the centroid of m and section A, I_c is the mass moment of inertia of m about its centroid, θ is the angular acceleration of m , and M is axle bending moment at section A. Here again, L is the wheel load and \ddot{z}_c is the vertical acceleration at the centroid of m . The wheel load instrumentation based on Equation 2 will be referred to as the bending-moment transducer.

A drawback of the shear-force transducer is that it produces a small strain-gauge electrical signal in comparison with what the bending-moment transducer produces. A drawback of the bending-moment transducer is that it is susceptible to errors caused by any tire side forces that may exist, and by possible variations of the length of moment arm d .

4.0 Experimental Hardware

Two types of tandem-axle suspension systems were tested; a drive-axle, air-bag suspension and a rubber-spring, walking-beam trailer suspension. The drive-axle suspension system was instrumented with strain-gauges sensitive to bending moment using the same procedure initially used by Woodrooffe et al. (ref. 2). Unsatisfactory calibration results obtained with the transducer on this suspension prompted the work reported in this paper.

The anomalies observed during the calibration of the drive-axle suspension initially were thought to be related to some interaction between drive-axle components (e.g., between the drive axle and axle housing). For this reason, the investigation was redirected to the instrumentation of the less complicated trailer suspension system. Each of its wheels was instrumented with two full strain-gauge bridges; one sensitive to bending moment, the other to shear force.

The bridge sensitive to bending moment consisted of two uniaxial strain gauges bonded to the top and bottom of the axle in the direction that made them sensitive to flexural strain of the axle resulting from an increase in vertical load (Figures 2). The bridge was completed with two dummy resistors so as to form a temperature-compensated electrical circuit.

The bridge sensitive to shear force consisted of two dual strain gauges. Each dual gauge consisted of two resistors sensitive to strain in a direction perpendicular to one another (Figures 2). The gauges were bonded so as to be sensitive to strain at a zenith angle of 45°. One dual gauge was bonded to the front face of the axle while the other was bonded to the rear. Together the dual gauges formed a temperature-compensated full bridge.

A uniaxial strain-gauge accelerometer was mounted right next to the wheel hub to measure vertical acceleration. The same accelerometer was used for both the bending-moment and shear-force transducers.

The calibrations were performed with NRC's experimental vehicle supported on a servo-hydraulic shaker facility (Figure 3). The facility consisted of four hydraulic actuators each equipped with a load cell for measuring vertical load. The load cells had been

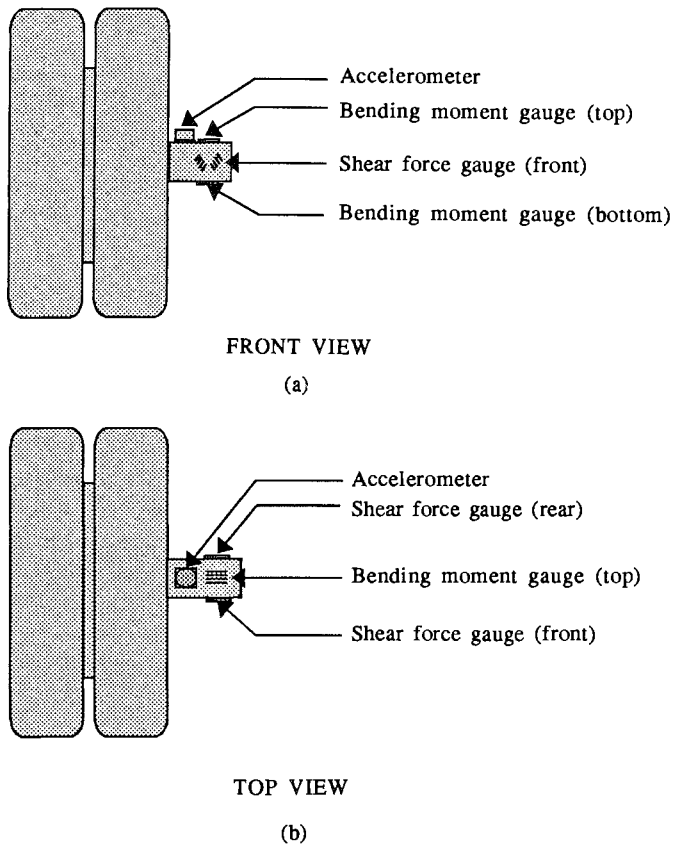


Fig. 2. Front and top views of dual wheel and axle stub showing the locations of the strain gauges

calibrated to first-order national standards by NRC's Institute for Aerospace Research. The vehicle's dual wheels were supported by wheel platforms fastened to the top of the load cells. Each wheel platform had a mass of 95 kg. Their inertia was taken into account during the calibration by means of accelerometers mounted on the platforms. The hydraulic-actuator displacements were measured from LVDT signals used for controlling the servo-hydraulic actuators.

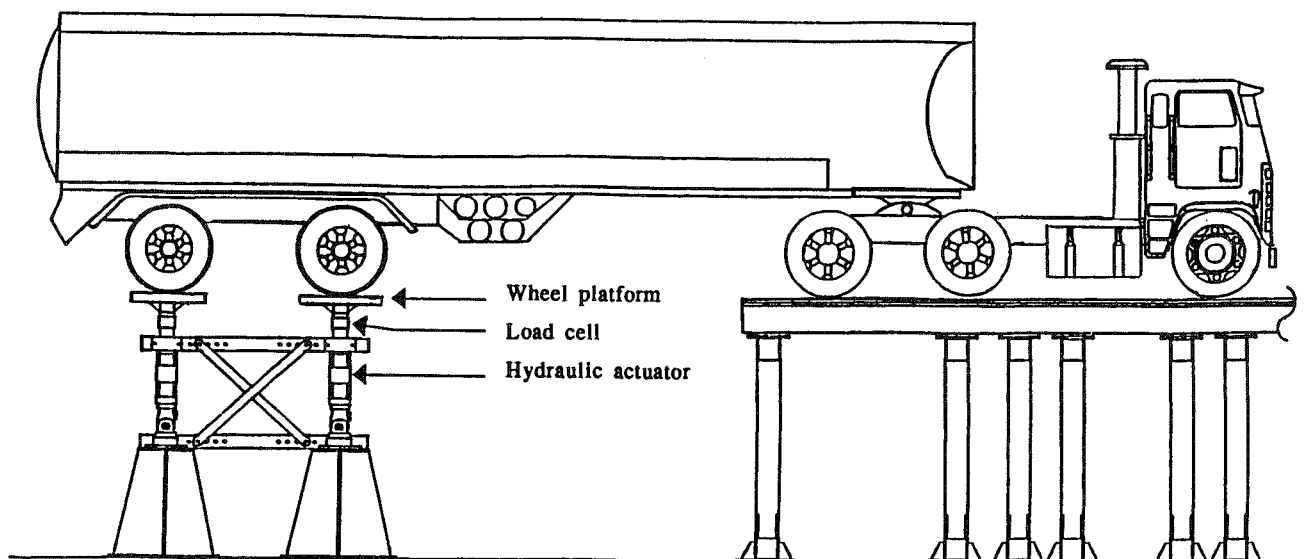


Fig. 3. NRC's experimental tractor-semitrailer on four post hydraulic shaker facility

A total of 24 channels was recorded at 750 samples/s/channel with a 20,000 sample/s, 16-bit data acquisition system. The time lapse between each reading for a given scan was equal to 1/20,000 th of a second. The electrical signals were filtered with 4-pole Butterworth filters with a cutoff frequency of 140 Hz.

The selection of the sampling rate was based primarily on the phase-shift effect that 4-pole Butterworth filters have on electrical signals. One of the requirements for the second phase of the NRC Project (an investigation into the spatial repeatability characteristics of dynamic wheel loads) is that wheel load signals corresponding to the sprung and unsprung mass modes of vibration not be altered by phase shifts of more than 15°. In order to meet this requirement a filter cutoff frequency of 140 Hz was necessary. The selected filters attenuate the amplitude of 375 Hz signals to approximately 2% of their original amplitude. According to the Nyquist criteria, when sampled at 750 samples/s, the recorded data will be contaminated by signals beyond 375 Hz due to aliasing effects. Given that 375 Hz signals were to be attenuated to 2% of their original amplitude, and that signals beyond 375 Hz were to be attenuated at a rate of 80 dB/decade, a sampling rate of 750 samples/s was considered adequate.

5.0 Static Calibration

A static calibration of the strain gauges was conducted by slowly lowering the tandem axle wheels onto the wheel platforms of the shaker facility while recording the strain gauge bridge and load cell signals. These calibrations were conducted five times in order to produce a statistical data base. Three calibrations were conducted at the beginning of the test programme and two at the end. A typical calibration curve is shown in Figure 4.

The calibration results are expressed in terms of the slope of the best fit line, hereafter referred to, as the shear-force and bending-moment calibration constants. The shear-force calibration constants are used during dynamic tests to convert the electrical signal from the shear-force bridges into shear force (parameter V in Equation 1) as required by the shear-force transducer. Similarly, the bending-moment calibration constants are used during dynamic tests to convert the electrical signal from the bending-moment bridges into units of force (the term M/d in Equation 2) as required by the bending-moment transducer.

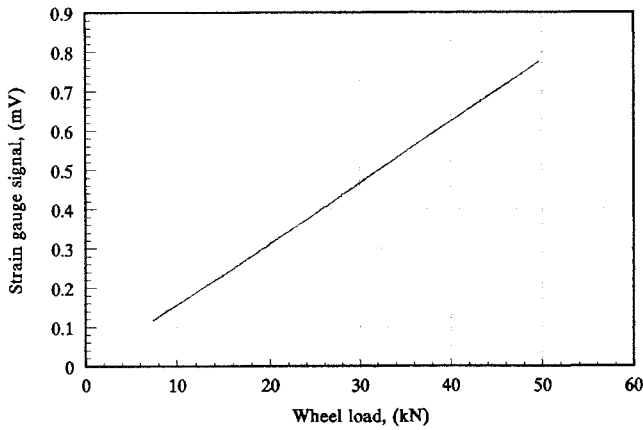


Fig. 4. Typical static calibration curve.

As noted, five calibration constants were generated for each of the eight strain-gauge bridges. The mean value for each of the eight bridges is listed in Tables 1 and 2. Also included in Tables 1 and 2 is the absolute value of the maximum difference between the mean calibration constant (for a given bridge) and the five individual calibration constants (for that same bridge). The maximum difference from the mean value was less than 0.5% for all of the eight bridges. The static calibration results also reveal that the bending-moment calibration constants are approximately 2.5 times greater than the shear-force calibration constants.

Table 1. Calibration constants for shear-force gauges

	Lead axle		Trailing axle	
	passenger side	driver side	passenger side	driver side
	mV/kN	mV/kN	mV/kN	mV/kN
mean	0.01557	0.01565	0.01571	0.01577
maximum variation from mean	0.00003	0.00008	0.00002	0.00003

Table 2. Calibration constants for bending-force gauges

	Lead axle		Trailing axle	
	passenger side	driver side	passenger side	driver side
	mV/kN	mV/kN	mV/kN	mV/kN
mean	0.0391	0.0376	0.0397	0.0375
maximum variation from mean	0.0001	0.0001	0.0002	0.0002

The accelerometers used on the axles and the wheel platforms were subjected to two-point calibrations (± 1 g). The accelerometer calibrations were repeated four times, twice at the beginning of the test programme and twice at the end. The results, summarized in Tables 3 and 4, indicate that the calibration constants for the axle accelerometers varied from the mean values by less than 1% and that the calibration constants for the platform accelerometers varied from the mean values and by less than 2%.

Table 3. Calibration constants for axle accelerometers

	Lead axle		Trailing axle	
	passenger side	driver side	passenger side	driver side
	mV/g	mV/g	mV/g	mV/g
mean	0.1107	0.1080	0.1118	0.1137
maximum variation from mean	0.0003	0.0008	0.0003	0.0006

Table 4. Calibration constants for platform accelerometers

	Lead axle		Trailing axle	
	passenger side	driver side	passenger side	driver side
	mV/g	mV/g	mV/g	mV/g
mean	0.1088	0.405	0.750	0.1095
maximum variation from mean	0.0016	0.002	0.003	0.0006

6.0 Dynamic Calibrations

The purpose of the dynamic calibrations is to determine the optimum value for inertial-force-related terms in Equations 1 and 2. For the shear-force transducer this term consists of the mass outboard of the strain gauges (m), while for the bending-moment transducer, the inertial terms consist of the effective mass $m\bar{y}/d$ and the additional term I_c/d .

Based on the assumption of a rigid axle, the vertical accelerations at the centroid of the mass outboard of the strain gauges can be calculated from

$$\ddot{z}_{ci} = (\ddot{z}_1 + \ddot{z}_2)/2 + (-1)^{i+1} \bar{Y}(\ddot{z}_1 - \ddot{z}_2)/\ell, \quad i=1, 2 \quad (3)$$

where subscripts 1 and 2 correspond to wheels 1 and 2 shown in Figure 5, \ddot{z}_{ci} is the acceleration at the centroid of m_i (the mass outboard of the strain gauges), \ddot{z}_1 and \ddot{z}_2 are the accelerations measured by the axle accelerometers, \bar{Y} is the distance between the centre of the axle and the centroid of m_i , and ℓ is the distance separating the two accelerometers on the axle. The angular acceleration of the axle and dual wheels is given by

$$\ddot{\theta} = (\ddot{z}_1 - \ddot{z}_2)/\ell \quad (4)$$

According to shear-force transducer theory (Equation 1), the wheel load, L_{si} , can be evaluated from

$$L_{si} = V_i - m_i \ddot{z}_{ci}, \quad i=1, 2 \quad (5)$$

Similarly, according to bending-moment transducer theory (Equation 2), the wheel load, L_{bi} , can be evaluated from

$$L_{bi} = (M/d)_i - (m\bar{y}/d)_i \ddot{z}_{ci} - (-1)^{i+1} (I_c/d)_i \ddot{\theta}, \quad i=1, 2 \quad (6)$$

As indicated in Section 4, the vertical force readings obtained from the load cells (mounted to the upper portion of the hydraulic-actuators) were corrected to account for the inertia of the wheel platforms. The mass of a single platform was 95 kg. Dynamic equilibrium of the vertical forces acting on the platform requires that

$$L_{ri} = L_{ci} + m_p \ddot{z}_{pi}, \quad i=1, 2 \quad (7)$$

where L_{ri} , referred to as the reference wheel load, is the wheel load as measured from the load cell reading (L_{ci}) and the wheel platform inertia ($m_p \ddot{z}_{pi}$). The platform is shown in Figure 6.

6.1 Dynamic calibrations - Part A

The terms $(m\bar{y}/d)_i$ and m_i were evaluated from tandem axle hop tests conducted on the shaker facility. Two types of axle hop motions were considered; one where both axles were sinusoidally excited in phase and the other where both axles were sinusoidally excited out-of-phase. Given that the test suspension system was of a walking beam type, the former axle hop motion will be referred to as "tandem axle hop" while the latter axle hop motion will be referred to as "tandem axle pitch". Under these test conditions the vertical acceleration values on both sides of the axles were equal, and thus Equations 5 and 6 reduced to the following:

$$L_{si} = V_i - m_i \ddot{z}_i, \quad i=1, 2 \quad (8)$$

and

$$L_{bi} = (M/d)_i - (m\bar{y}/d)_i \ddot{z}_i, \quad i=1, 2 \quad (9)$$

Every term on the right side of Equations 7 to 9, with the exception of the two inertial terms $(m\bar{y}/d)_i$ and m_i , was measured either prior to or during the axle hop and axle pitch tests. The optimum value for $(m\bar{y}/d)_i$ and m_i was obtained by a computer iteration process which sought to minimize the difference between L_{si} and L_{ri} , and L_{bi} and L_{ri} . Although the tandem axle group was excited in hop and in pitch over a frequency range of 1 to 18 Hz, the optimum values for the inertial terms was obtained from the response of the system corresponding to the unsprung masses' natural frequencies. The natural frequency corresponding to tandem axle hop was approximately 12.5 Hz while the natural frequency corresponding to tandem axle pitch was closer to 12 Hz

As shown in Tables 5 and 6, the effective mass $(m\bar{y}/d)_i$ is significantly lower than is m_i . The results shown in Table 6 are in close agreement with results produced by Woodrooffe et al. for identical wheels and similar strain gauge positions. Whereas the results presented in Table 6 reveal that $(m\bar{y}/d)_i$ has an mean value of 250 kg and a standard deviation of 20 kg, Woodrooffe et al. reported a mean value of 235 kg and a standard deviation of 10 kg.

According to the results presented in Table 5, the mean value and standard deviation for m_i are 310 and 10 kg, respectively. The results obtained for $(m\bar{y}/d)_i$ and m_i imply that the moment arm ratio \bar{y}/d is approximately equal to 0.8. This is plausible given that a significant portion of the wheel assembly's mass (the wheel drum and brake assembly) is in board of the dual-wheel centre. The actual mass of the dual wheels plus the estimated mass of the axle stub was previously found to be 300 kg (ref. 2).

The most likely reason for the large variation in the values of $(m\bar{y}/d)_i$ found in Table 6 is explained in the second paragraph of Section 8.

Table 5. Optimum values for m_i .

Axle hop test	Lead axle		Trailing axle	
	passenger side	driver side	passenger side	driver side
	kg	kg	kg	kg
Axles in phase	296	302	312	325
Axles out-of-phase	307	308	300	318

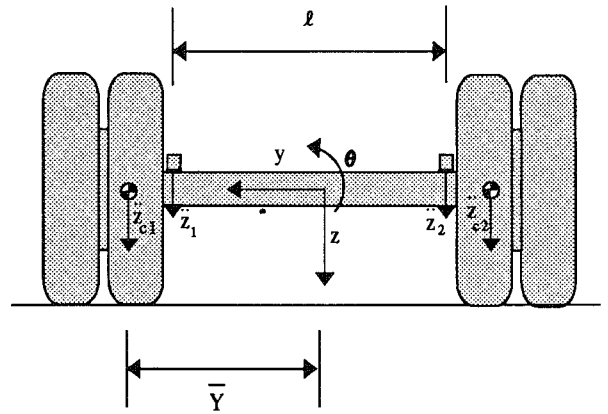


Fig. 5. Instrumented axle

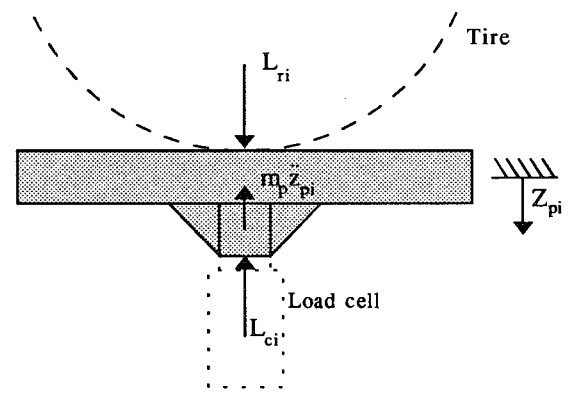


Fig. 6. Free body diagram of wheel platform

Table 6. Optimum values for $(m\bar{y}/d)_i$.

Axle hop test	Lead axle		Trailing axle	
	passenger side	driver side	passenger side	driver side
	kg	kg	kg	kg
Axles in phase	259	205	260	283
Axles out-of-phase	248	241	248	265

The final values used as the masses and effective masses are presented in Table 7. Because tandem axle pitch motion predominates over tandem axle bounce (as revealed by experimental results), the final values used were weighted towards the axle pitch motion.

Table 7. Final dynamic calibration values form m_i and $(m\bar{y}/d)_i$.

	Lead axle		Trailing axle	
	passenger side	driver side	passenger side	driver side
	kg	kg	kg	kg
m_i	305	305	305	320
$(m\bar{y}/d)_i$	255	230	255	275

The accuracy of both types of wheel load instrumentation is illustrated in Figures 7 to 14, where the reference wheel load (L_{ri}) and the load measured by the wheel load transducers (L_{si}) and (L_{bi}) are plotted against frequency. Also included on the graphs is a curve for the difference between the wheel load derived from the shaker facility's load cells and the wheel load measured by the on-board instrumentation. Because the difference in wheel load often consisted of a complex wave form, its magnitude is expressed in terms of the standard deviation of the time-history. In order to compare properly the difference in wheel load with the actual wheel load measurements, the reference and on-board wheel loads are also expressed in terms of the standard deviation of their time-histories.

The results shown in Figures 7 to 14 are representative of those obtained in general. The peaks in Figures 7 and 8 correspond to the trailer pitch frequency (≈ 2.8 Hz) and the tandem axle hop frequency (≈ 12.5 Hz); the peaks in Figures 9 and 10 correspond to the tandem axle pitch frequency (≈ 12 Hz); and the peaks in Figures 11 and 12 correspond to the roll frequency of the tractor's air suspension (≈ 0.5 Hz) and the roll frequency of the trailer suspension (≈ 0.8 Hz). No specific mode of vibration was excited from the motion whose results are shown in Figures 13 and 14.

The results presented in Figures 7 to 10 reveal that the two wheel-load transducers performed very well under both the tandem axle hop and tandem axle pitch motions. Not so, however, when the axle group was subjected to tandem axle roll excitation with both axles excited in phase. For this motion, the bending-moment transducer's performance was highly unsatisfactory (Figure 12). Similar unsatisfactory bending-moment transducer results were obtained when the tandem axles were subjected to axle roll excitation with both axles excited out-of-phase (Figure 14).

The time history corresponding to the peak value of Figure 12 is shown in Figure 15. Similarly unsatisfactory results were obtained with the tractor air suspension instrumented with the bending-moment wheel load transducers. The results for the air suspension are not shown here, but, as mentioned earlier, it is they which prompted the investigation reported in this paper. The authors conclude, therefore, that axle roll motion produces sufficiently high side forces to severely contaminate the signals produced by the bending-moment transducer. The contamination exists whether axle roll motion induces sprung mass roll (when both axles roll in phase, Figure 12) or whether axle motion does not induce the sprung mass to roll (when both axles roll out-of-phase, Figure 14). As will be argued in Section 7.0, the results shown in Figures 12 and 14 are not as significant as they appear to be.

6.2 Dynamic calibrations - Part B

The second part of the dynamic calibration consisted of evaluating the remaining inertial-force-related term. Equation 6 can be rewritten as follows:

$$L_{bi} = (M/d)_i - (m\bar{y}/d)_i \ddot{z}_{ci} - (-1)^{i+1} (I_c/t d)_i (\ddot{z}_1 - \ddot{z}_2), \quad i = 1, 2$$

The optimum value for $I_c/t d$ was evaluated by a computer iteration process which sought to minimize the difference between L_{bi} and L_{ri} from tests involving excitation of the tandem axles in roll motion at approximately 12 Hz. The iteration process led to unsatisfactory results, namely, the term $I_c/t d$ was found to vary between -15 and -40 kg. An estimated upper limit for this term is 75 kg. The estimate is based on a hypothetical dual wheel whose mass is homogeneously distributed throughout its volume. Hence, both at low and high frequencies, the bending-moment transducer leads to unsatisfactory results.

The wheel load response to tandem axle roll excitation is shown in Figures 16 and 17 for peak-to-peak actuator displacements of 0.5 cm. (The results shown in Figures 11 and 12 were produced for a

0.9 cm peak-to-peak displacements.) Note how the magnitude of the wheel load measured by the bending-moment transducer exceeds that of the reference wheel load at frequencies above 9 Hz. As argued in the next section, the inaccuracies present at high frequencies are believed to be more important than those at lower frequencies.

Whittemore, in his study, resolved the acceleration at the centroid of the dual wheel from the acceleration measured by two accelerometers, as described by Equation 3. Woodrooffe et al., on the other hand, instrumented only one side of the experimental vehicle and, consequently, approximated the acceleration at the centroid of the dual wheel as being equal to that measured by a single accelerometer.

The shaker tests conducted to determine the optimum value of $I_c/t d$ also served to establish the importance of resolving the acceleration at the centroid of the dual wheel from two accelerometers, in order to account for axle roll. The wheel load time-histories shown in Figures 18 and 19 were generated from tests involving 12 Hz axle roll excitation. The curves in Figure 18 consist of the reference wheel load and the wheel load measured by the shear-force transducer for the case where the acceleration at the centroid of the dual wheel is assumed equal to the acceleration measured by the accelerometer adjacent to the shear gauges (i.e., the effect of axle roll is disregarded). The curves in Figure 19 consist of the same reference wheel load as in Figure 18, but in this case the wheel load from the shear-force transducer was evaluated by resolving the acceleration at the centroid of the dual wheel using Equation 3 (i.e., the effect of axle roll are considered).

As revealed in the next section, axle roll motion during normal vehicle operating conditions is indeed measurable.

7.0 Road Tests

The signals produced by the two types of wheel-load transducers were compared during road tests. The experimental vehicle was driven over a smooth road, at speeds of 75, 85, and 95 km/h, and over a very rough road, at speeds of 60, 70, and 80 km/h. Each of these tests was conducted three times, for a total of 18 tests. The results from one of the tests were rejected due to a false start.

The coefficients of variation of the wheel load, often referred to as the Dynamic Load Coefficient (DLC), measured by the shear-force transducers are plotted against nominal speed for all 17 successful road tests (Figure 20). The DLCs were evaluated using two different approaches, namely, (i) by using Equation 3 to resolve the acceleration at the centroid of the dual wheel (i.e., the effects of axle roll were considered), and (ii) by assuming that $\ddot{z}_{ci} = \ddot{z}_i$ (i.e., the effects of axle roll were not considered). The contribution of axle roll to the magnitude of the DLC was found to increase in percentage as the dynamic activity of the wheel load increased. For example, for DLCs of less than 0.2 the contribution of axle roll was less than 0.5% while for DLCs of 0.4 the contribution of axle roll was as much as 2.5%.

The DLCs were also calculated from the bending-moment transducers with the approach used by Woodrooffe et al., that is, only the accelerometer reading adjacent to the strain gauges was considered. The results are shown in Figure 21. Also included in Figure 21 are the DLCs measured with the shear-force transducer for the case where axle roll is considered. The readings from the bending-moment transducers were found to exceed those from the shear-force transducer by 3% on average with a standard deviation of about 1.5%. The percentage difference between the readings for the two types of transducers was found to be independent of the magnitude of the DLC.

Power spectral density analysis of the road test data revealed that no appreciable level of frequency content existed below 2.5 Hz. Also,

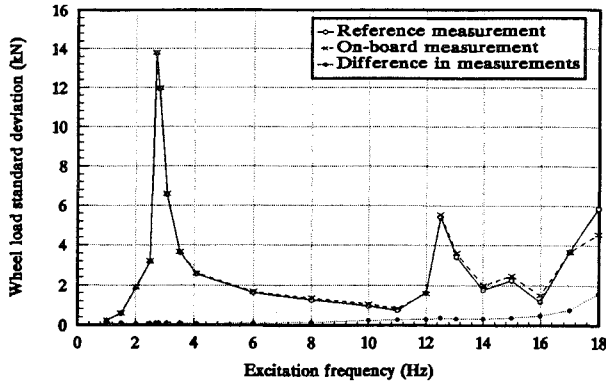


Fig. 7. Shear-force transducer results for tandem axle hop excitation, 0.25 cm peak-to-peak actuator displacement.

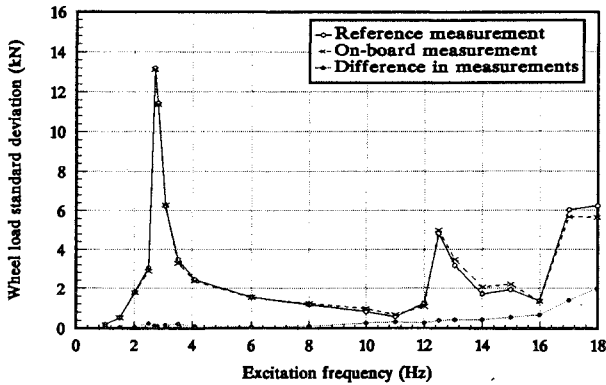


Fig. 8. Bending-moment transducer results for tandem axle hop excitation, 0.25 cm peak-to-peak actuator displacement.

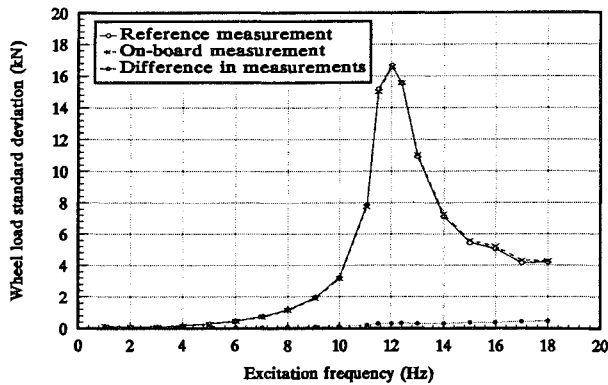


Fig. 9. Shear-force transducer results for tandem axle pitch excitation, 0.25 cm peak-to-peak actuator displacement.

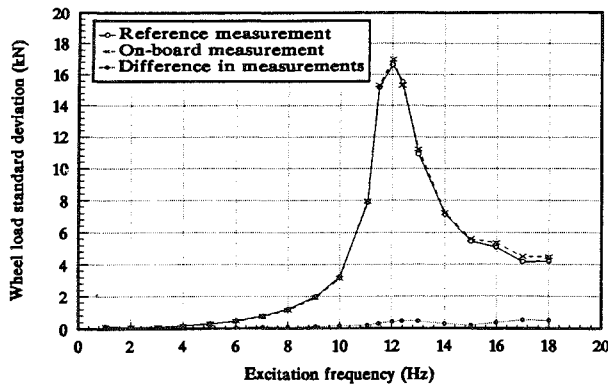


Fig. 10. Bending-moment transducer results for tandem axle pitch excitation, 0.25 cm peak-to-peak actuator displacement.

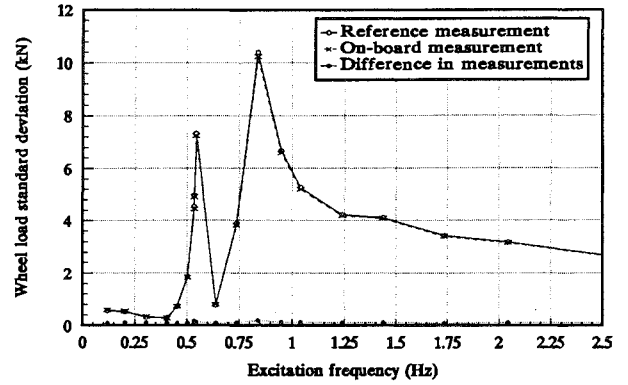


Fig. 11. Shear-force transducer results for tandem axle roll excitation, 0.90 cm peak-to-peak actuator displacement.

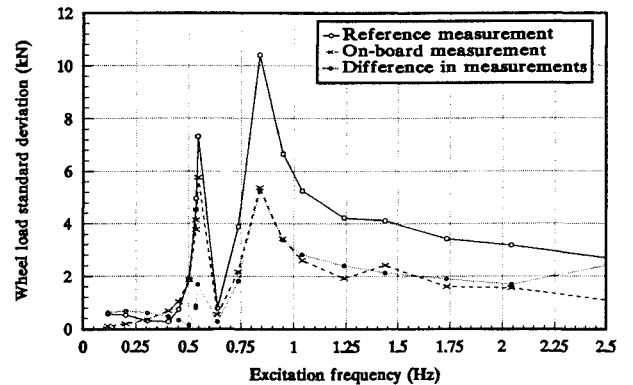


Fig. 12. Bending-moment transducer results for tandem axle roll excitation, 0.90 cm peak-to-peak actuator displacement.

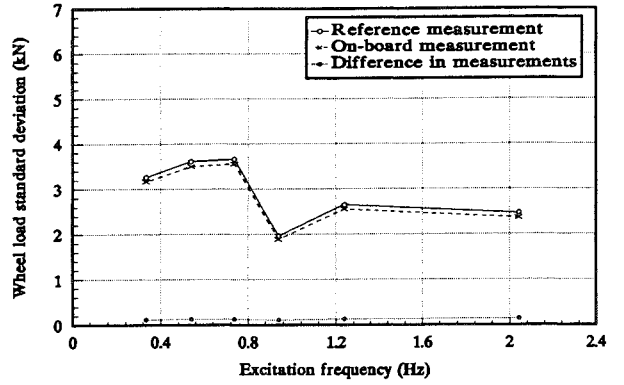


Fig. 13. Shear-force transducer results for tandem axle roll (out-of-phase) excitation, 2.5 cm peak-to-peak actuator displacement.

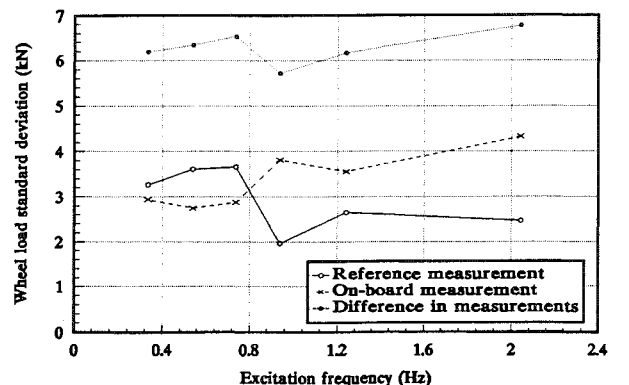


Fig. 14. Bending-moment transducer results for tandem axle roll (out-of-phase) excitation, 2.5 cm peak-to-peak actuator displacement.

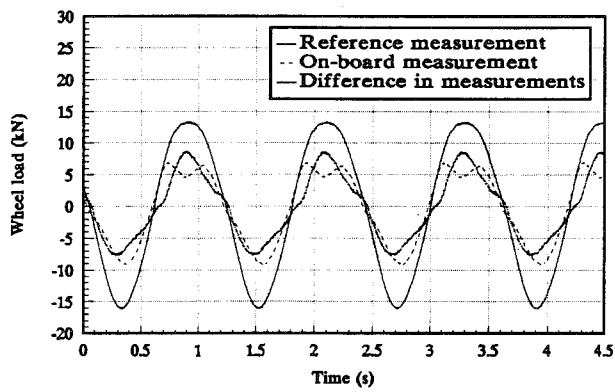


Fig. 15. Time domain results for tandem axle roll excitation at 0.8 Hz (the sprung mass' highest roll frequency).

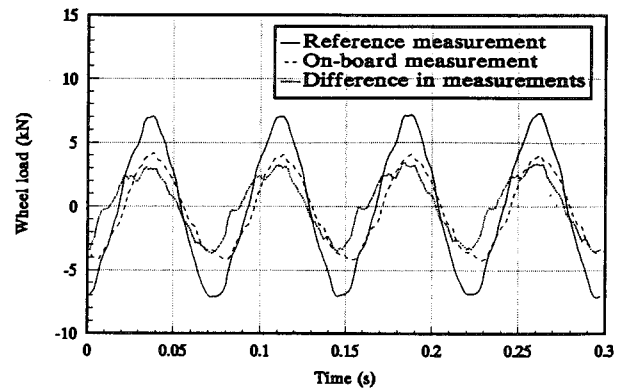


Fig. 18. Effect of axle roll not considered. Results from shear-force transducer.

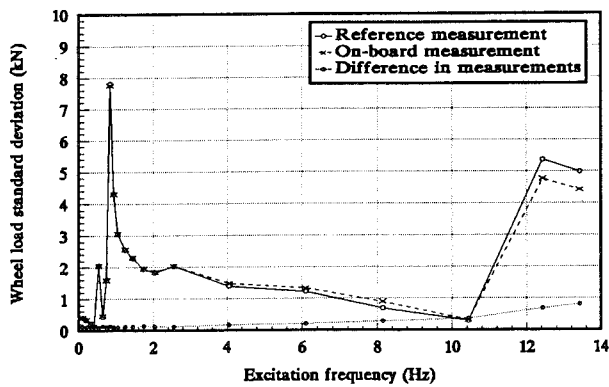


Fig. 16. Shear-force transducer results for tandem axle roll excitation, 0.50 cm peak-to-peak actuator displacement

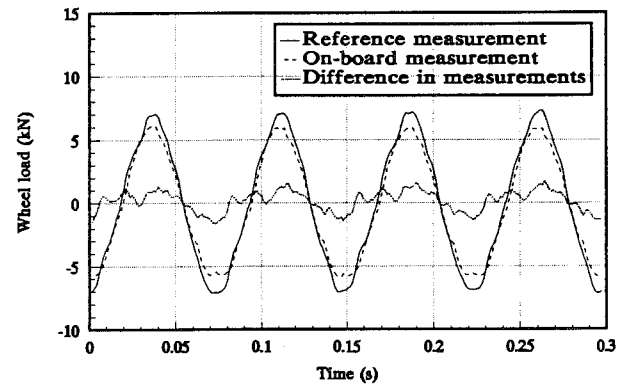


Fig. 19. Effect of axle roll considered. Results from shear-force transducer.

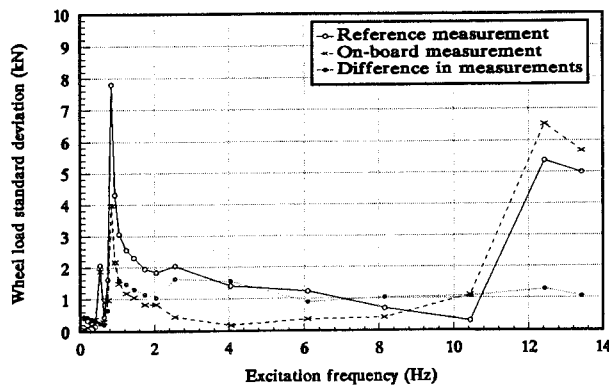


Fig. 17. Bending-moment transducer results for tandem axle roll excitation, 0.50 cm peak-to-peak actuator displacement.

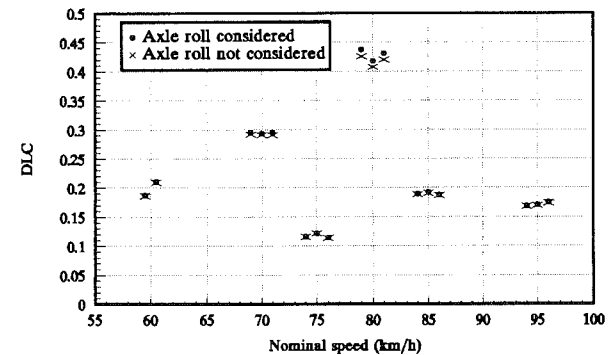


Fig. 20. Effect of axle roll inertia on DLCs.

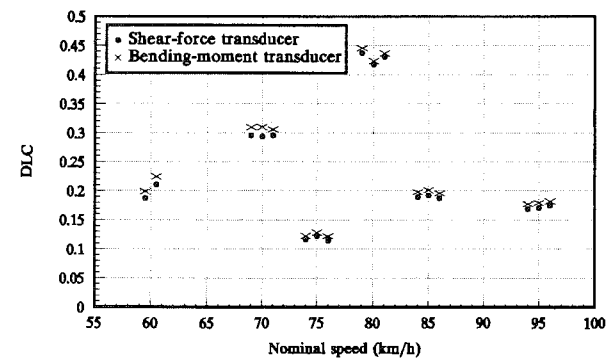


Fig. 21. Comparison of DLCs from shear-force transducer with axle roll considered against DLCs from bending-moment transducer without axle roll considered.

the power level associated with the sprung and unsprung masses is slightly higher for the bending-moment transducer than it is for the shear-force transducer. It follows, therefore, that the anomalies associated with the roll frequencies of the trailer (0.5 and 0.8 Hz, Figure 12) played no significant role in producing the difference in DLC values obtained for the two wheel load transducers.

The higher power level found for the bending-moment transducer at the unsprung mass frequencies of 12 Hz is consistent with the anomalies that were observed in the shaker tests when the axles were subjected to axle roll excitation. The higher power level found for the bending-moment transducer at the sprung mass frequency of 2.8 Hz is believed to be related to the fact that the static calibrations were conducted on a non-rolling tire. When a vertical load is applied to an axle whose wheels are rolling, the tires are free to move laterally to compensate for axle flexure. On the other hand, when a vertical load is applied to an axle whose wheels are

not rolling, the tires are prevented from moving laterally by side forces directed towards the centre of the axle. These forces have the effect of decreasing the bending-moment calibration constant which in turn will have the effect of overestimating the wheel load generated by rolling wheel. For example, if, during the static calibration, a 1 kN increase in wheel load produces a 0.10 mV increase signal output, then an equivalent increase in wheel load of 1 kN during a road test will produce a signal output of, say, 0.11 mV which will be interpreted from the bending-moment static calibration constant as being an increase in wheel load of 1.1 kN.

8.0 Conclusions

The axle-roll-related anomalies encountered during the dynamic calibrations for the bending-moment transducer are significant. These anomalies are considered to outweigh the advantage inherent in the bending-moment transducer, namely, that it produces higher signal output per unit of vertical force than does the shear-force transducer. Also, the difference in DLC measurements obtained during the road tests are most likely the result of deficiencies of the bending-moment transducer with respect to axle roll motion and to a slightly erroneous static calibration constant. Although the differences between the two types of transducers is relatively small during normal highway operating conditions, the shear-force transducer is considered to be superior to the bending-moment transducer.

The large standard deviation obtained for the effective mass ($m\ddot{y}/d$)_i in Table 6 (20 kg), is also believed to be the result of contamination of the bending-moment transducer signals caused by axle roll. Although the tests in which the effective mass was evaluated were intended to be pure tandem axle hop and pitch, examination of the experimental data shows that there was, nevertheless, an appreciable amount of axle roll.

Finally, axle roll excitation is significant enough during severe highway operating conditions to take into account the rotational inertia of the dual wheel. This entails the use two accelerometers to resolve the angular acceleration of the wheel.

References

1. Sweatman P.F. "A Study of Dynamic Wheel Forces in Axle Group Suspensions of Heavy Vehicles", Special Report No. 27, Australian Road Research Board, 1983
2. Woodroffe J.H.F., LeBlanc P.A., and LePiane K.R. "Effects of Suspension Variations on the Dynamic Wheel Loads of a Heavy Articulated Highway Vehicle", Technical Report, Vehicle Weights and Dimensions Study, Volume 11, Roads and Transportation Association of Canada (RTAC), 1986
3. Whittemore A.P., Pollack D.E., Schultz P.C., and Wiley J.R. "Dynamic Pavement Loads of Heavy Highway Vehicles", National Cooperative Highway Research Program, Report 105, 1970
4. Cantieni R. "Dynamic Load Tests on Highway Bridges in Switzerland", Report No. 211, Swiss Federal Laboratories for Materials Testing and Research (EMPA), Dübendorf, Switzerland, 1983
5. Hopkins R.C. and Boswell H.H. "Methods for Measuring Load Transfer Through Vehicle Tires to the Road Surface", Division of Highway Transport Research, Bureau of Public Roads, 1957